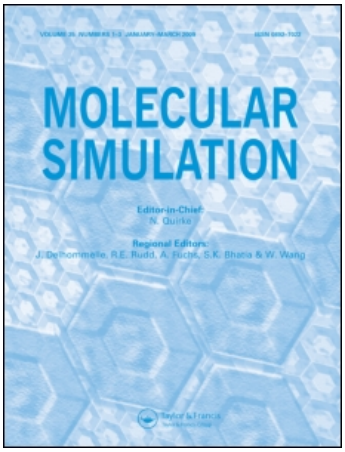

Molecular Simulation
Publication details, including instructions for authors and subscription information:
http://www.informaworld.com/smpp/title~content=t713644482

A molecular dynamics study on intermediate structures during transition from amorphous to crystalline state

F. A. Celik[a]; S. Ozgen[a]; A. K. Yildiz[a]
[a] Physics Department, Faculty of Arts & Sciences, Firat University, Elazig, Turkey

To cite this Article Celik, F. A. , Ozgen, S. and Yildiz, A. K.(2006) 'A molecular dynamics study on intermediate structures during transition from amorphous to crystalline state', Molecular Simulation, 32: 6, 443 — 449
To link to this Article: DOI: 10.1080/08927020600779889
URL: http://dx.doi.org/10.1080/08927020600779889

Molecular Simulation, 32, No. 6, 15 May 2006, 443–449

Taylor & Francis
Taylor & Francis Group

A molecular dynamics study on intermediate structures during transition from amorphous to crystalline state

F.A. CELIK, S. OZGEN and A.K. YILDIZ*

Physics Department, Faculty of Arts & Sciences, Firat University, 23119 Elazig, Turkey

(Received February 2006; in final form April 2006)

Molecular dynamics (MD) simulations are carried out for model aluminium with 500, 864, 1372 and 2048 atoms interacting with Sutton-Chen version of embedded atom method (SCEAM) based on many body interactions. The systems equilibrated in an FCC structure have, first, been melted and then solidified with specifically selected single cooling rate which forms unstable amorphous state in the system. The local structures of the system have been analysed by bond orientational order parameters to distinguish the simple structures in the systems. The radial distribution functions (RDF) and atomic coordinates have also been analysed for determining the local structural properties. It has been observed that the phase sequences of the systems, except for those of the 2048 atoms, are FCC → Liquid → Amorphous → Mixed Crystal. Types of the crystals in the mixed state depend on the number of the atoms in the system. The final phase of the system with 2048 atoms is amorphous state.

Keywords: Molecular dynamics; Embedded atom method; Solidification; Local order

1. Inroduction

The systems such as amorphous, microcrystalline metals and alloys prepared by rapid cooling processes possess various excellent properties such as high strength and magnetization, and their macroscopic properties are mainly determined by investigating the microstructures. In order to develop effective methods for controlling the properties, it is very important to understand the evolution mechanisms of microstructure in forming amorphous and microcrystalline metals, but at this level of development it is not an easy task to do experimentally. In the past several years, the structural properties of small clusters have been studied by using a variety of techniques [1–3]. In particular, experimental difficultly in the area can be overcome using MD simulations [4].

MD simulations based on the interatomic interactions are widely used to research the structural properties of metals or its alloys and amorphous systems. The embedded atom method (EAM) originally proposed by Daw and Baskes [5,6] based on many body interactions has been used confidently in MD simulations on metallic systems and used widely to solve the many problems in bulk, surface and interface of metals and alloys [7–10]. However, the EAM applications on the liquid and amorphous phases of metallic systems are increasing from day to day [11–15].

The structural properties, such as clusters and lattice cells, of the simulated solids or liquids have recently been investigated by three dimensional bond orientational orders calculated from the spherical harmonics. An investigation of the bond orientational order parameters in liquids and glasses had been studied comprehensively by Steinhardt et al. [16], applying it to the simulation of supercooled Lennard-Jones liquids and metallic glasses. Subsequently, it has been used to determine the degree of crystalline and icosahedral (ICOS) order during melting and nucleation [17–19], and the local orientational symmetrical features of the clusters in liquid or amorphous metals [20–22]. There are also a few simulation studies on the Al system during rapid cooling processes [23,24]. Generally, it has been observed from these studies that the systems with different number of atoms exhibit a different transition mechanism during structural transformation from amorphous to crystalline solids [13], and FCC- and HCP-like structures occur in the final structures [21]. However, it can be seen that FCC- and HCP-like structures have not been investigated extensively.

*Corresponding author. Email: ayildiz@firat.edu.tr

Molecular Simulation
ISSN 0892-7022 print/ISSN 1029-0435 online © 2006 Taylor & Francis
http://www.tandf.co.uk/journals
DOI: 10.1080/08927020600779889

In this study, we have purposed to investigate the metal clusters, especially FCC- and HCP-like structures, in aluminium during transformation from amorphous state to crystalline state by using MD simulations based on SCEAM. The structure of the obtained solid and liquid phases has been analysed by using radial distribution function (RDF). The properties of local structure in liquid and solid phases of aluminium have also been analysed with the bond orientational order parameters. The remainder of the study is divided into four sections. In the first section, the theoretical background of EAM is briefly presented. In the second the simulation application of the MD is explained. In the third, the calculations of the bond orientation order parameters for the systems are given. In the forth, we present the results and discussion, and in the last section the article ends with a short conclusion.

2. Interatomic potential

In the EAM formalism, the binding energy of atom i in a crystal with N atoms is a sum of contributions from the pair potential and embedding potential functions. Various approaches have been applied to define EAM functions [25–28]. Among those, the SCEAM approach is one of the simple approaches of the EAM, which has defined by incorporating the essential band character of metallic cohesion [27]. In this approach the total crystal energy is calculated from

$$E_{\mathrm{T}} = \varepsilon \sum_{i=1}^{N} \left[\frac{1}{2} \sum_{j \neq i}^{N} \left(\frac{a}{r_{ij}} \right)^{n} - c\sqrt{\bar{\rho}_i} \right], \tag{1}$$

$$\bar{\rho}_i = \sum_{j \neq i}^{N} \left(\frac{a}{r_{ij}} \right)^{m}. \tag{2}$$

Here, r_{ij} is the distance between atoms i and j, c is a positive dimensionless parameter, ε is a parameter in dimension of energy, a is the lattice constant, and m and n are positive integers, which are determined by fitting to the experimental properties of material such as lattice constant (a), cohesive energy (E_{c}), and bulk modulus (B_{m}). The potential parameters for Al have been taken as $a = 4.05$ Å, $\varepsilon = 33.147$ meV, $c = 16.399$, $n = 7$ and $m = 6$ from [27].

3. Simulation procedure

In this study, the MD method developed by Parrinello and Rahman [29], which allows anisotropic volume change and so it can produce a NPH or NPT statistical ensembles, has been used.

In the simulation studies, the equations of motion of the system were numerically solved by using the velocity version of Verlet algorithm with an integration step size of 2.35 fs. Potential energy functions were truncated at a distance of 8.1 Å ($2a_0$). Initial MD cell were constructed on a lattice with FCC unit cell for the systems of 500, 864, 1372 and 2048 atoms. The periodic boundary conditions were applied on the three dimensions of the MD cell. Time averages of the thermodynamic and structural properties of the systems in each simulation run were determined for 8000 integration steps following the equilibration of 2000 steps. The temperature of the systems has been controlled by rescaling the atomic velocities at every five integration steps. The simulation processes were carried out as follows:

First, the simulation runs were applied for getting the equilibration of the system under zero pressure at 300 K, and then the temperature was increased from 300 to 700 with 50 K increment in each run of 10,000 integration steps. At 700 K temperature, it has been observed that the system has a liquid phase, and so an extra 10,000 steps were waited at 700 K to obtain relatively mixed liquid phase. Second, the liquid phase was cooled down from 700 to 100 K with 100 K increment in each run of 10,000 steps. The cooling rate was calculated as 4.25×10^{12} K/s for the simulation runs of cooling process.

The structures of the systems in solid and liquid phases were examined using the RDF,

$$g(r) = \frac{V}{N^2} \left\langle \frac{\sum_i n_i(r)}{4\pi r^2 \Delta r} \right\rangle. \tag{3}$$

Here, $g(r)$ is the probability of finding of an atom in the range between r and $r + \Delta r$, the angular bracket denotes the time average. N is the number of atoms, $n_i(r)$ is the coordination number around atom i in the range from r to $r + \Delta r$.

4. Bond orientational order parameters

The local structures of the atoms in the MD cell are determined from the calculation of the bond orientational order parameters [13,16,30]. In this formalism, the nearest neighbours of each atom in the MD cell, which constitute a cluster, is obtained by using a cut-off distance taken from the minimum of the RDF between the first and the second maximum. The spherical coordinates of each bond in the cluster is calculated from, which are associated with a set of numbers in terms of the spherical harmonics,

$$Q_{lm}(\mathbf{r}) \equiv Y_{lm}(\theta(\mathbf{r}), \phi(\mathbf{r})) \tag{4}$$

where $Y_{lm}(\theta, \phi)$ are spherical harmonics, and $\theta(\mathbf{r})$ and $\phi(\mathbf{r})$ are the polar and azimuthal angles of the bond measured with respect to some reference frame. Hence, the local bond order parameters can be worked out by averaging equation (4) over the number of the bonds (N_{b}) in the cluster

$$\bar{Q}_{lm} \equiv \frac{1}{N_{\mathrm{b}}} \sum_{\mathrm{bonds}}^{N_{\mathrm{b}}} Q_{lm}(\mathbf{r}). \tag{5}$$

Table 1. The values of bond order parameters of some typical clusters.

Cluster	Q_4	Q_6	$\hat{W}_4$	$\hat{W}_6$
ICOS	0	0.66332	0	−0.16975
FCC	0.19094	0.57452	−0.15931	−0.01316
HCP	0.09722	0.48476	0.13409	−0.01244
DHCP	0.15221	0.49618	0.03494	−0.01160
FCT	0.6182	0.70403	0.02917	−0.04790
Liquid	0	0	0	0

In order to make the order parameters invariant with respect to rotations of the reference frame, second-order invariants (Q_l) and third-order invariants (W_l), respectively, are worked out from the equations below

$$Q_l \equiv \left[\frac{4\pi}{2l+1}\sum_{m=-l}^{l}\left|\bar{Q}_{lm}\right|^2\right]^{1/2} \tag{6}$$

$$W_l \equiv \sum_{\substack{m_1,m_2,m_3 \\ m_1+m_2+m_3=0}} \begin{bmatrix} l & l & l \\ m_1 & m_2 & m_3 \end{bmatrix} \times \bar{Q}_{lm_1}\bar{Q}_{lm_2}\bar{Q}_{lm_3}, \tag{7}$$

where the parameters in square brackets are the Wigner 3j-symbols. The reduced order parameters do not depend strictly on the definition of the nearest neighbours, and can be calculated from

$$\hat{W}_l \equiv \frac{W_l}{\left[\sum_{m=-l}^{l}\left|\bar{Q}_{lm}\right|^2\right]^{3/2}}. \tag{8}$$

It is, in general, known that Q_6 and $\hat{W}_6$ is adequate to identify the structures of clusters confidently. In this calculation in addition to these two parameters, we have also worked out Q_4 and $\hat{W}_4$ for more accurate determinations. The bond order parameters values have been obtained for FCC, HCP, "double hexagonal cubic packed" (DHCP), face centred tetragonal (FCT), ICOS, and liquid structures, which are given in table 1.

5. Results and discussion

First of all, the melting temperatures of the systems have been obtained before the simulation studies on heating and cooling of the systems. To determine the melting temperature (T_m), the variation of the cohesive energy with temperature, which is called caloric curve, was plotted for zero pressure. From this plot, the melting temperature was obtained as 500 ± 50 K in an error of −46% considering the experimental data of 933.5 K [31]. A few methods for the determination of T_m have been used in MD simulations [4,32]. It has been known that the caloric curve method used in this study always gives a lower melting point than experimental data, although it is the simplest ones [7,32], and also the SCEAM gives a lower melting point for the systems of small number of atoms [33]. For this reason, the obtained T_m value can be accepted for our studies to determine the liquid structure.

The obtained results have been plotted for the systems only with 864 and 2048 atoms since the results of those with 500, 864 and 1372 atoms are very close to each other qualitatively.

The RDFs obtained at different temperatures during heating and cooling processes are given in figure 1(a) and (b) for two systems. The RDF curves have been plotted by using the same $g(r)$ scale at all temperatures. Since the peak locations for 300 K satisfy the certain peak locations at 1, $\sqrt{2}$, $\sqrt{3}$, $\sqrt{4}$, $\sqrt{5}$, etc. times of r_0 in an ideal FCC unit cell, the model systems have an FCC unit cell under zero pressure at initial condition. So the RDF curves at 300 K for initial FCC structures are in agreement with the experimental structure of aluminium [31]. Also, at 500 K the structures are liquid [15].

As shown in the figure 1(a) and (b), the second peak width of the RDF curves for cooled states at 300 K is increasing with increasing temperature, so it can be said that the second nearest neighbour coordination split during solidification of material. The splitting of these peaks at 300 K is also observed by other researchers for

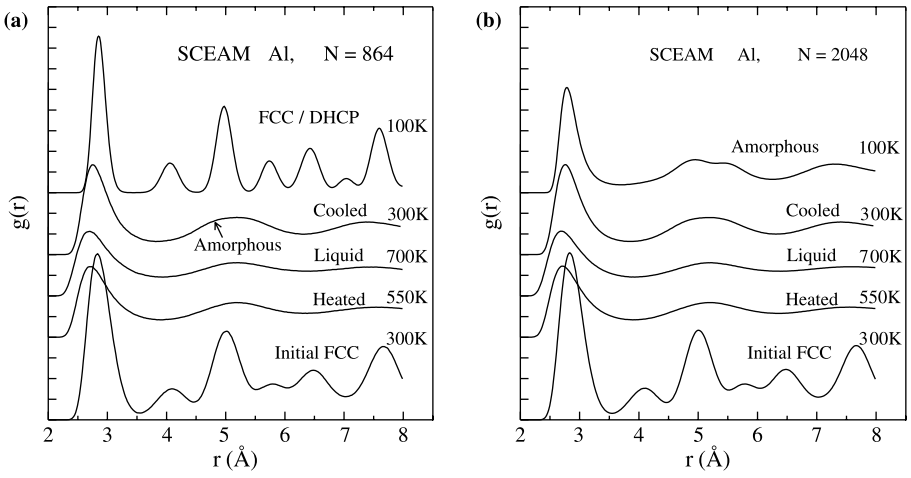

Figure 1. The RDF curves of the systems with (a) 864 and (b) 2048 atoms.

aluminium and different amorphous materials, and it is defined as a common feature of amorphous materials [34]. In the figure 1(a), it has been shown that the amorphous structure of the system become the stable crystal structure with decreasing temperature or during the equilibrating at 100 K, but for the system of 2048 atoms holds in a stable amorphous structure at 100 K (figure 1(b)). In fact, different methods are suggested to determine the glass transition temperature (T_g) which is observed widely in amorphous materials. According to one of these definitions, known as Wendt-Abraham ratio [8], the g_{min}/g_{max} ratios of the RDF curves at different temperatures are calculated and then plotted versus temperature [10,15,21]. Here, g_{min} is the first minimum value, and g_{max} is the first maximum value of the RDF curve. In the graph two lines having two different slopes occur, and the glass transition temperature is taken as intersection point of these lines. The graphs of g_{min}/g_{max} ratios versus temperature obtained in this study for two systems are given in figure 2(a) and (b). From this figures, it can be said that the T_g value of the system with 864 atoms has not been determined as clearly as that of the system with 2048 atoms, but it is estimated roughly as 300 K. Although the glassy transition attempts in the systems with low number of atoms have been observed at 300 K, these systems have not been successful to keep in the glassy state and they have become crystalline solids.

In order to investigate the unit cells or clusters occurred in the crystalline solids attempting the glassy transition, Q_l and $\hat{W}_l$ from equations (6)–(8) were first worked out for each clusters centred at each atom i for $l = 4$ and 6 at different temperatures, and then averaged for each values of l over all atoms in the MD cell. The average values of Q_6 and $\hat{W}_6$ have been given in figure 3(a)–(d) for the systems with 864 and 2048 atoms. As expected, in heating process the variation of bond order parameters of all systems with temperature show a similar behaviour with increasing the number of atoms in the MD cell. For temperature below 550 K the internal structure remains nearly FCC unit cells, which shows the similar behaviour as in Ref. [13]. On the other hand, the case in cooling process is completely different, which can, obviously, be seen on panels (a)–(d) of figure 3. The values of Q_6 given on panels (a and c) consistent with each other as temperature decreasing down to 300 K, but then below this temperature differ from each other with the number of atoms. This difference is also seen for $\hat{W}_6$ values on panels (b and d). For temperature below 300 K the system with 864 atom attempt to transform from liquid to amorphous state, but it did not stable in amorphous state. The decrease of $\hat{W}_6$ values after the maximum at 200 K shows that the system has a tendency to form crystalline structure for 864 atoms. However, as the number of atoms is increased, i.e. $N = 2048$, the system remains at amorphous phase on panel (d). These arguments can also be seen on the curves of RDF.

Moreover, another calculation has been done for $\hat{W}_4$ values for two different cases of atomic number which is presented in figure 4 (a) and (b). As seen on panel (a) that values of $\hat{W}_4$ did not change during the heating process for both cases while a significant change with the number of atoms appeared on panel (b) during the cooling process. In other words, the result showed that in heating the values of $\hat{W}_4$ started from approximately -0.9 and increased up to 0. This result is in agreement with the literatures in Ref. [13,18,21]. On the other hand, in figure 4 (b) it is seen that the values for the system with 2048 atoms slightly decrease in negative region, although it increase unexpectedly up to a 0.008 value passing through to positive region for the system with 864 atoms. The expected final value in the crystalline solid must be negative because the solid may include many FCC unit cells or clusters, which have a value of -0.15931 for $\hat{W}_4$. Although it was considered in the first case that the HCP or DHCP clusters could give rise to this increase, later it was realized that the increase could be caused by the FCT or DHCP clusters when the real space atomic coordinates were investigated.

The DHCP and HCP unit cells have been shown in figure 5. Although the simplest pattern of atomic stacking, AB, corresponds to the (mono) HCP structure, a four-period sequence, ABAC, leads to the DHCP [35,36]. In fact, the existence of the DHCP unit cells can not be proved by analysing the RDF curve, in particular where FCC unit cells become dense, because most peaks of the RDF curve of the FCC cells superpose those of the DHCP

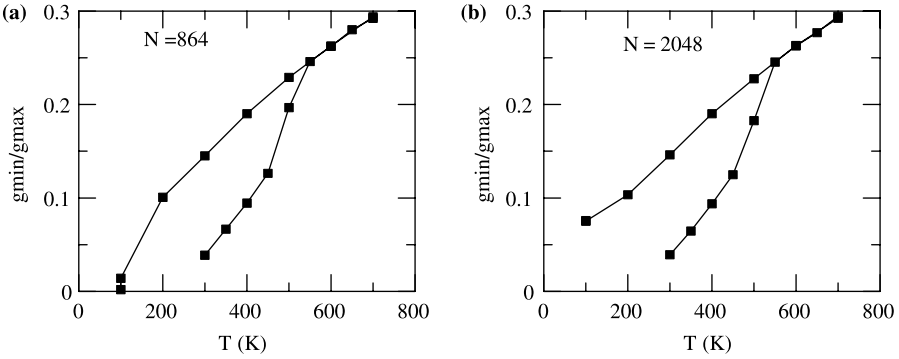

Figure 2. Wendt-Abraham ratios versus temperature for the systems with (a) 864 and (b) 2048 atoms.

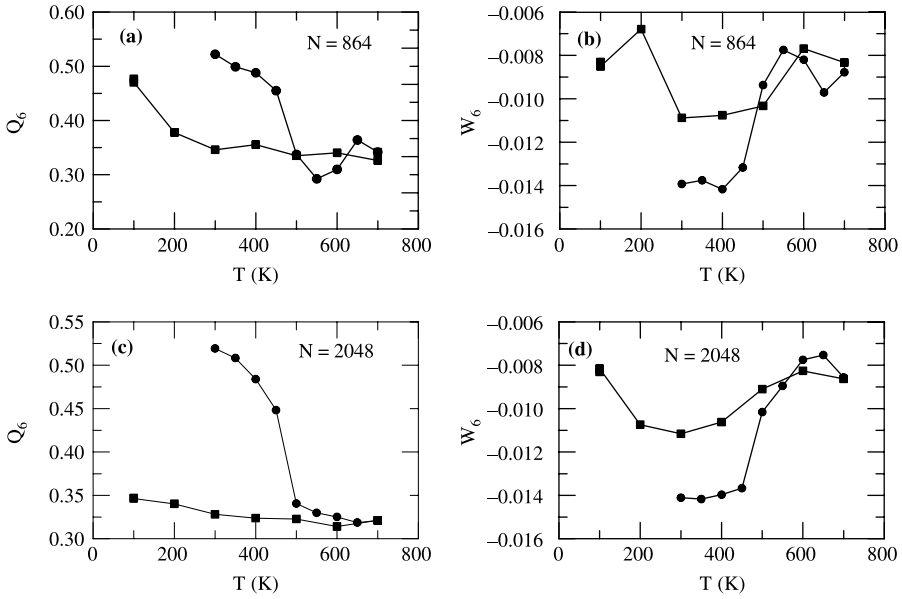

Figure 3. The average values of Q_6 and $\hat{W}_6$ versus temperature for the systems with 864 and 2048 atoms. Circle- and square-shaped symbols represent the heating and cooling processes, respectively.

unit cells. To overcome this problem we believe that the bond orientational order parameters are useful technique to determine whether the simulated structures involve DHCP cells or not. Therefore Q_4, Q_6, $\hat{W}_4$ and $\hat{W}_6$ values have been calculated, which are given in table 1.

The existence of the DHCP unit cells in the simulated structures can be confirmed by analysing the changes in the values of order parameter $\hat{W}_4$with temperature since it produces the best value for the DHCP cells as seen from table 1. In the present study, the $\hat{W}_4$ order parameter has been used to distinguish the FCC, HCP and DHCP or other unit cells in the final structures. Figure 6 (a)–(f) show Q_4 and $\hat{W}_4$ distributions at initial and final states for all the systems except for the system with 500 atoms because it produces nearly similar results as that of 864 atoms.

As seen in the figure 6 (a),(c) and (e), the systems have the same distributional properties in initial states at 300 K which represent that most part of their structures contain FCC unit cells. In the final states at 100 K given in figure 6 (b),(d) and (f), on the other hand, there is no trace of similarity among the distributional properties. In other words, there are conspicuous differences representing system properties such as amorphous state with 2048 atoms and crystalline states of the other systems. Moreover, there are also systematic differences between two crystalline systems with 864 and 1372 atoms as seen in figure 6 (b) and (d). It has been observed that the two solids have two different heaps of data. The first heap for the system of 864 atoms occurs in the interval of $0.15 < Q_4 < 0.20$ at $0 < \hat{W}_4 < 0.035$, and the second is in $0.20 < Q_4 < 0.25$ at the same $\hat{W}_4$ as the first. Also, the first heap for the system with 1372 atoms is within the interval of $-0.14 < \hat{W}_4 < -0.05$ and $0.11 < Q_4 < 0.17$, and the second is within $0 < \hat{W}_4 < 0.05$ and the same interval for Q_4. It can be said from the results in table 1 that the first heap for the system with 1372 atoms corresponds to the FCC structure, and the second one is neither an agent of FCC nor HCP structure, but it can be a signature of DHCP structure, which was confirmed from the investigation of the real space coordinates of atoms. Hence, the second heap for the system with 864 atoms has also been interpreted in the same way with very little exception for the data interval of Q_4. Also, the first heap has been explained as that it could be a signature of FCT cells due to both the increase of Q_4 value up to 0.25 and the positive value of $\hat{W}_4$. Finally, the

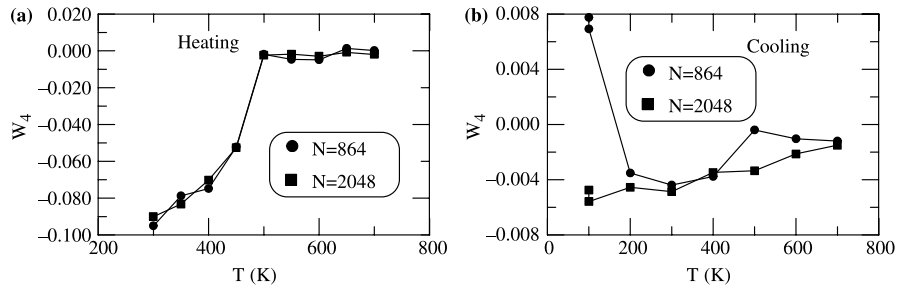

Figure 4. The changes of $\hat{W}_4$ with temperature for the systems with 864 and 2048 atoms. (a) Heating and (b) cooling processes.

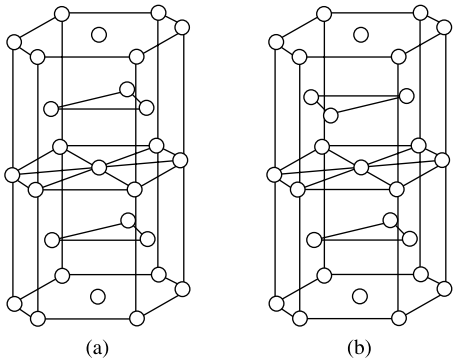

Figure 5. Close-packed structures: (a) HCP and (b) DHCP [34].

system with 2048 atoms at the final state was unable to form crystalline structure.

In the gold nanorods with different number of atoms, and shape, the structural transformations from FCC to HCP and the mechanism of crystal growth from amorphous atomic layers was investigated by Wang and Dellago [13] using MD simulations and bond orientational order parameters. They focused on the mechanism of the morphological and structural transition emerges during melting of the models, and found that their models with different number of atoms exhibited different structural transitions. In order to distinguish FCC from HCP structures they also made some definitions on Q_4 and $\hat{W}_4$ values, such as FCC ($Q_4 > 0.17$ and $\hat{W}_4 < -0.10$) and HCP ($Q_4 < 0.13$ and $\hat{W}_4 > 0.07$). Hence, according to their definitions, the FCC structures in our study are not consisting of completely ideal FCC unit cells, but they might have some tetragonally deformed cubic cells. In addition, it has been observed that the systems with different number of atoms exhibit a different transition mechanism during structural transformation from amorphous to crystalline solids, as observed in Ref. [13]. However, it is known that final structure formed in a solid–solid phase transition depends both on annealing time and temperature at high temperature phase. The same situation can also occur in the systems solidified from liquid phase, which will be interesting to investigate in a future study.

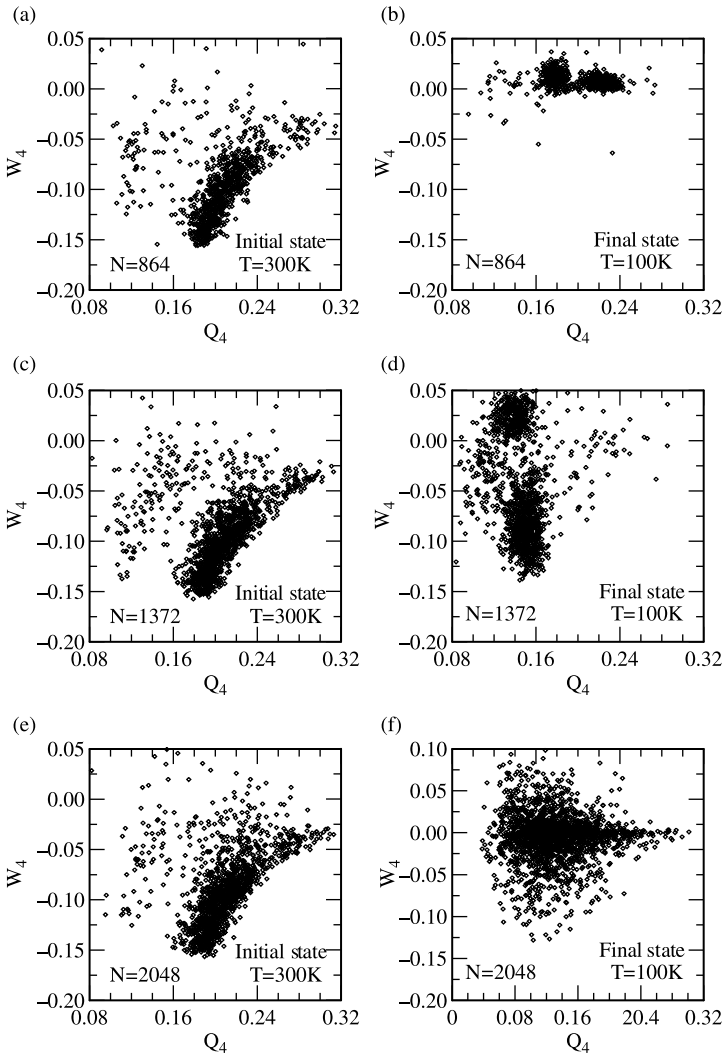

Figure 6. Q_4 and $\hat{W}_4$ distributions for the systems with 864, 1372 and 2048 atoms for the initial and final states.

6. Conclusion

In this communication, MD simulation calculation, based on the SCEAM method for atomic interactions, was performed on some aluminium systems with different number of atoms to determine the local structures from the RDF and the calculation of the bond orientational order parameters. In the calculations it was achieved to some interesting results that the final structures of the systems not only consist completely of pure FCC unit cells, but also DHCP and FCT unit cells, and the structures in the final state depend strongly on the number of atoms in the system. The bond orientational order parameters for $l = 4$ and 6 were, in particular, worked out to determine the structure of DHCP. In connection with this statement, it is interesting to note that, to the best of our knowledge, there exists no literature to clarify that the structures modelled with the SCEAM consist of DHCP unit cells. In this view, we believe that this study is the first one involving the SCEAM method. However, we must note that the detailed investigation of the transformation mechanisms such as cooling rate for solidification and annealing time is under consideration for a future communication.

References

[1] D.R. Nelson, J. Toner. Bond-orientational order, dislocation loops, and melting of solids and smectic-A liquid crystals. *Phys. Rev. B.*, **24**, 363 (1981).

[2] D.R. Nelson. Order, frustration, and defect in liquids and glasses. *Phys. Rev. B.*, **28**, 5515 (1983).

[3] J.D. Honeycutt, H.C. Andersen. Molecular dynamics study of melting and freezing of small Lennard-Jones clusters. *J. Phys. Chem.*, **91**, 4950 (1987).

[4] J.M. Haile. *Molecular Dynamics Simulation, Elementary Methods*, John Wiley & Sons, Canada (1992).

[5] M.S. Daw, M.I. Baskes. Semiempirical quantum mechanical calculation of hydrogen embrittlement in metals. *Phys. Rev.*, **17**, 1285 (1983).

[6] M.S. Daw, M.I. Baskes. Embedded-atom method: derivation and application to impurities, surfaces, and other defects in metals. *Phys. Rev. B.*, **29**, 6443 (1984).

[7] Y. Gurler, S. Ozgen. The calculations of P-T diagrams of Ni and Al using molecular dynamics simulation. *Mater. Lett.*, **57**, 4336 (2003).

[8] Y. Qi, T. Cagin, Y. Kimura, W.A. Goddard III. Molecular-dynamics simulations of glass formation and crystallization in binary liquid metals: Cu–Ag and Cu–Ni. *Phys. Rev. B.*, **59**, 3527 (1999).

[9] C. Kuiying, S. Xianwei, Z. Xiumu, L. Yiyi. Rapid solidification of Cu-25at.%Ni alloy: molecular dynamics simulations using embedded atom method. *Mater. Sci. Engin.*, **A214**, 139 (1996).

[10] C. Kuiying, L. Hongbo, L. Xiaoping, H. Qiyong, H. Zhuangqi. Molecular dynamics simulation of local structure of aluminium and copper in supercooled liquid and solid state by using EAM. *J. Phys. Condens. Matter*, **7**, 2379 (1995).

[11] T.M. Brown, B. Adams. EAM calculations of the thermodynamics of amorphous copper. *J. Non-Crystalline Solids*, **180**, 275 (1995).

[12] L. Wang, X. Bian, J. Zhang. Structural simulation of amorphization and crystallization in liquid metals. *J. Phys. B. At. Mol. Opt. Phys.*, **35**, 3575 (2002).

[13] Y. Wang, C. Dellago. Structural and morphological transitions in gold nanorods: a computer simulation study. *J. Phys. Chem. B.*, **107**, 9214 (2003).

[14] G. Zhou, Q. Gao. Molecular dynamics simulation of the solidification of liquid gold nanowires. *Solid State Commun.*, **136**, 32 (2005).

[15] S. Ozgen, E. Duruk. Molecular dynamics simulation of solidification Kinetics of aluminium using Sutton-Chen version of EAM. *Mater. Lett.*, **58**, 1071 (2004).

[16] P.J. Steinhardt, D.R. Nelson, M. Ronchetti. Bond-orientational order in liquids and glasses. *Phys. Rev. B.*, **28**, 784 (1983).

[17] P.R. Ten Wolde, M.J. Ruiz-Montero, D. Frenkel. Numerical calculation of the rate of crystal nucleation in a Lennard-Jones system at moderate undercooling nucleus. *J. Chem. Phys.*, **104**, 9932 (1996).

[18] L. Hui, D. Feng, B. Xiufang, W. Guanghou. Molecular dynamics study of icosahedral ordering and defect in the Ni_3 Al liquid and glasses. *Chem. Phys. Lett.*, **354**, 466 (2002).

[19] Y. Wang, S. Teitel, C. Dellago. Melting and equilibrium shape of icosahedral gold nanoparticles. *Chem. Phys. Lett.*, **394**, 257 (2004).

[20] L. Wang, L. Haozhe, C. Kuiying, H. Zhuangqi. The local orientational orders and structures of liquid and amorphous metals Au and Ni during rapid solidification. *Physica B.*, **239**, 267 (1997).

[21] U. Gasser, A. Schofield, D.A. Weitz. Local order in a supercooled colloidal fluid observed by confocal microscopy. *J. Phys. Condens. Matter.*, **15**, S375 (2003).

[22] L. Hui, F. Pederiva. Structural study of local order in quenched lead under high pressures. *Chem. Phys.*, **304**, 261 (2004).

[23] C.S. Liu, G. Zhu, J. Xia, D.Y. Sun. Cooling rate dependence of structural properties of alumunium during rapid solidifacition. *J. Phys. Condens. Matter.*, **13**, 1873 (2001).

[24] K.J. Dong, R.S. Liu, A.B. Yu, R.P. Zou, J.Y. Li. Simulation study of the evolution mechanism of clusters in a large-scale liquid Al system during rapid cooling processes. *J. Phys. Condens. Matter.*, **15**, 743 (2003).

[25] M.W. Finnis, J.E. Sinclair. A Simple empirical N-body potential for transition metals. *Philos. Mag. A.*, **50**, 45 (1984).

[26] R.A. Johnson. Alloy model with the embedded-atom method. *Phys. Rev. B.*, **39**, 12554 (1989).

[27] A.P. Sutton, J. Chen. Long-range Finnis-Sinclair potentials. *Philos. Mag. Lett.*, **61**, 139 (1990).

[28] M.I. Baskes. Determination of modified embedded atom method parameters for nickel. *Mater. Chem. Phys.*, **50**, 152 (1997).

[29] M. Parrinello, A. Rahman. Polymorphic transitions in single crystals: a new molecular dynamics methodi. *J. Appl. Phys.*, **52**, 7182 (12).

[30] C. Chakravarty. Bond orientational order in atomic clusters. *Mol. Phys.*, **100**, 3777 (2002).

[31] C. Kittel. *Introduction to Solid State Physics*, John Wiley & Sons, Inc., New York (1986).

[32] S.K. Nayak, S.N. Khanna, B.K. Rao, P. Jena. Thermodynamics of small nickel clusters. *J. Phys. Condens. Matter*, **10**, 10853 (1998).

[33] Y. Qi, T. Cağın, W.L. Johnson, W.A. Goddard III. Melting and crystallization in Ni nanoclusters: the mesoscale regime. *J. Chem. Phys.*, **115**, 385 (2001).

[34] I. Skauvik, J.P. Hansen, T. Matthey. Dynamics of clustering in a binary Lennard-Jones material. Model. Simul. Mater. Sci. Eng., **8**, 665 (2000).

[35] A. Mujica, A. Rubio, A. Munoz, R.J. Needs. High-pressure phases of group-IV, III–V, and II–IV compounds. *Rev. Mod. Phys.*, **75**, 863 (2003).

[36] M. Prem, G. Krexner, O. Blaschko. Investigation of the two martensitic phase transitions hcp-dhcp and dhcp-fcc in Co-0.85 at %Fe by neutron scattering. *Mater. Sci. Engin.*, **A273–A275**, 491 (1999).